Impact of Ekman Pumping on the Meridional Coherence of the AMOC

Fraser, Neil J.; Fox, Alan D.; Cunningham, Stuart A.

Published in:
Geophysical Research Letters
Publication date:
2025

AGU ADVANCING EARTH AND SPACE SCIENCES

Geophysical Research Letters

RESEARCH LETTER
10.1029/2024GL108846

Impact of Ekman Pumping on the Meridional Coherence of the AMOC

Neil J. Fraser[1], **Alan D. Fox**[1], **and Stuart A. Cunningham**[1]

[1]The Scottish Association for Marine Science, Oban, UK

Abstract The effect of wind-induced vertical velocity on the meridional coherence of Atlantic meridional overturning circulation (AMOC) is examined using theory, observations, and a numerical model. Two cases are considered: (a) the AMOC computed in depth coordinates and (b) the AMOC computed in isopycnal coordinates. In depth space, the difference between the AMOC at different latitudes is largely explained by vertical transport across the 1000 m depth surface induced by Ekman pumping. In density space, this difference is explained by Ekman-driven heave of the neutral surface separating the upper and lower limbs. This adiabatic "sloshing" changes the relative volumes of the upper and lower AMOC limbs, obscuring the distribution and advection of the diapycnal transports which characterize the AMOC.

Plain Language Summary The Atlantic meridional overturning circulation (AMOC) is classically viewed as a continuous "conveyor" transporting warm water northward in its upper limb and cold water southward in its lower limb. It is natural to assume, then, that fluctuations in the AMOC strength are synchronous across latitude. However, observations from the last decade have drawn this interpretation into question, as the subtropical and subpolar AMOC show no evidence of temporal coherence. Here, we demonstrate that much of this lack of coherence can be explained by vertical velocities induced by wind over the North Atlantic.

Key Point:

- Lack of meridional coherence in observed Atlantic meridional overturning circulation can largely be explained by Ekman pumping

Correspondence to:

N. J. Fraser,
neil.fraser@sams.ac.uk

Citation:

Fraser, N. J., Fox, A. D., & Cunningham, S. A. (2025). Impact of Ekman pumping on the meridional coherence of the AMOC. *Geophysical Research Letters*, *52*, e2024GL108846. https://doi.org/10.1029/2024GL108846

Received 18 FEB 2024
Accepted 9 NOV 2024

Author Contributions:

Conceptualization: Neil J. Fraser, Alan D. Fox
Data curation: Stuart A. Cunningham
Formal analysis: Neil J. Fraser, Alan D. Fox
Funding acquisition: Stuart A. Cunningham
Investigation: Neil J. Fraser, Alan D. Fox
Methodology: Neil J. Fraser, Alan D. Fox
Project administration: Stuart A. Cunningham
Supervision: Stuart A. Cunningham
Visualization: Neil J. Fraser
Writing – original draft: Neil J. Fraser
Writing – review & editing: Neil J. Fraser, Alan D. Fox, Stuart A. Cunningham

1. Introduction

The Atlantic meridional overturning circulation (AMOC) is classically viewed as a continuous "conveyor" transporting warm water northward in its upper limb and cold water southward in its lower limb. It is natural to assume, then, that fluctuations in the AMOC strength are synchronous across latitude. However, observational results from the last decade (Fu et al., 2023; Moat et al., 2020) have drawn this interpretation into question, as the subtropical and subpolar AMOC show no evidence of temporal coherence (Figures 1 and 2).

Fraser et al. (2024) examine the vertical transport processes responsible for the depth-space overturning observed at both the RAPID (Moat et al., 2020) and OSNAP (Fu et al., 2023) arrays (Figure 1). Fraser et al. (2024) find that on seasonal to decadal time scales observed variability in the AMOC at each trans-atlantic section is dominated by Ekman pumping through the 1000 m depth surface integrated over the basins to the north of each respective section. Since the region of this surface north of OSNAP is a subset of the region north of RAPID, this suggests that differences between the RAPID and OSNAP time series are dominated by the Ekman pumping integrated over the complement of this subset, that is, the region of the 1000 m depth surface between the RAPID and OSNAP arrays.

Given the near-equivalence of the depth- and density-space AMOC at RAPID, together with the high level of temporal coherence between the depth- and density-space AMOC at OSNAP (Figure 2), it is likely that the same vertical transport processes are also responsible for the apparent lack of meridional coherence in density-space AMOC. Han (2023b) uses the term "sloshing" to describe the adiabatic change in the relative volumes of the upper and lower density classes which obscures the diapycnal component of the AMOC signal. Using a self-consistent ocean reanalysis, Han (2023a) computes isopycnal motion directly from the density field and finds excellent agreement with meridional differences in the density-space AMOC. He speculates that this sloshing is dominated by Ekman pumping.

In this paper, we examine the role of wind stress in upsetting the meridional coherence of the observed AMOC. We compute vertical transports from Ekman pumping on the interface between the upper and lower AMOC limbs in both depth and density space, and compare to the difference between the AMOC at RAPID

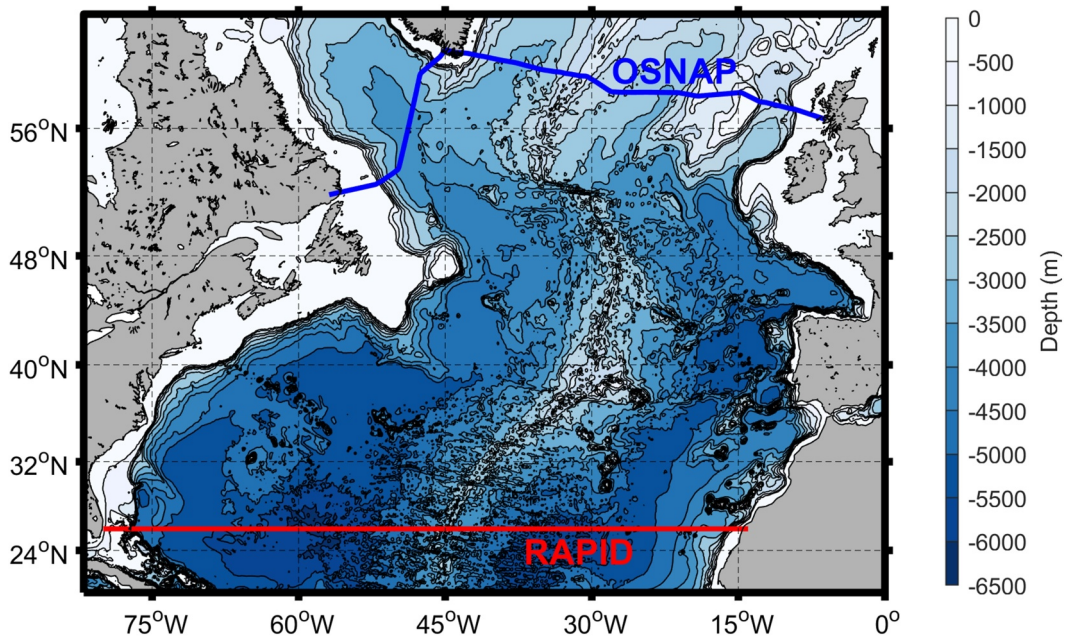

Figure 1. Bathymetric map of the North Atlantic indicating the locations of the RAPID and OSNAP sections.

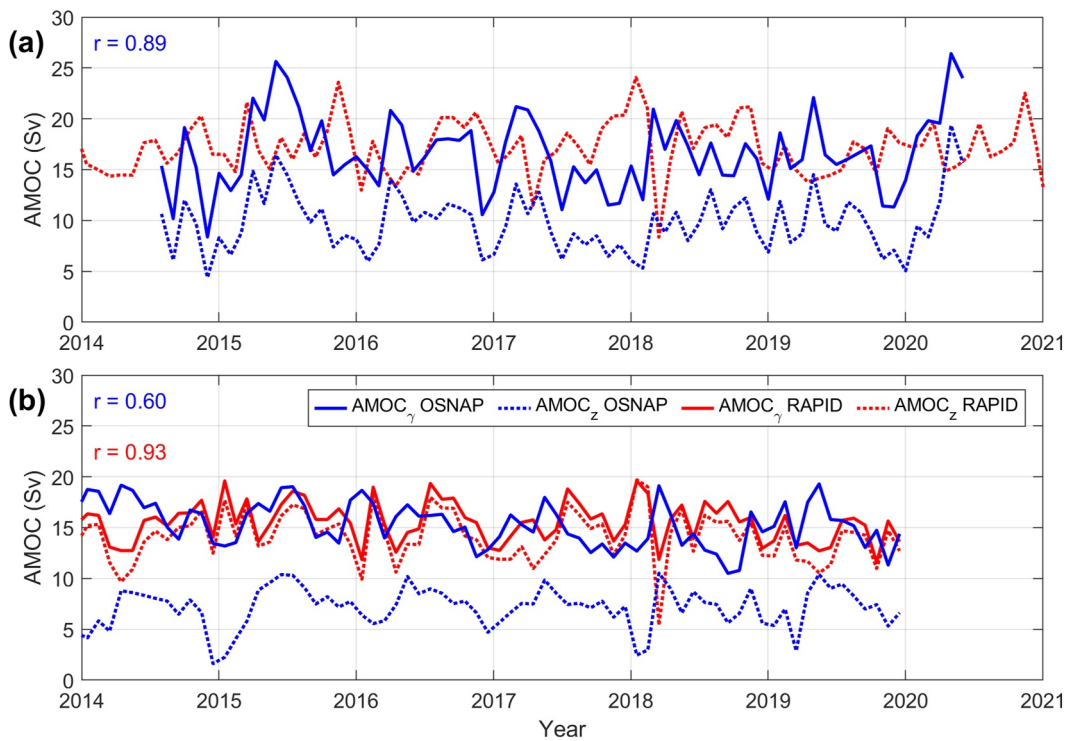

Figure 2. Time series for the AMOC at the subtropical RAPID section and the subpolar OSNAP section based on (a) observations from the OSNAP and RAPID arrays and (b) VIKING20X model output. Correlation between depth and density space AMOC at the OSNAP/RAPID sections is shown in blue/red text. The density-space AMOC at RAPID is available in the model only.

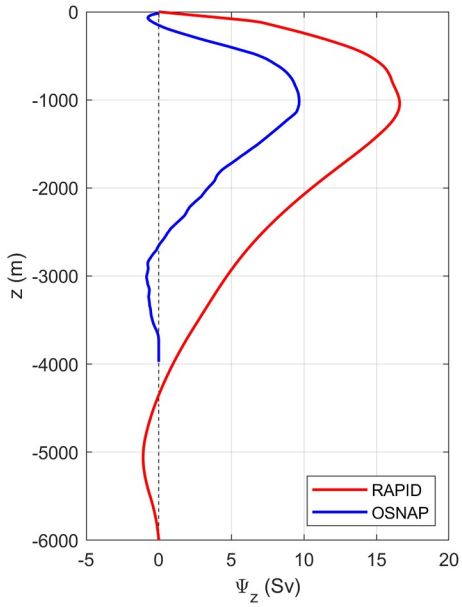

Figure 3. Time-mean overturning stream function Ψ_z in depth-coordinates observed at the RAPID and OSNAP arrays. In each case the maximum overturning (AMOC_z) occurs at a depth of $z = -1000$ m.

and that at OSNAP. We analyze output from various observation-based products as well as a high-resolution simulation of the North Atlantic Ocean, and interpret our results in the context of both the depth-space and density-space AMOC.

2. Depth Space

Consider A to be the region of the $z = -1000$ m surface bounded by the RAPID and OSNAP sections. Given that maximum overturning at both the RAPID and OSNAP sections occurs at a depth of $z = -1000$ m (Figure 3), each of these AMOC time series represents horizontal transport into the volume beneath the surface A (Figure 4). By continuity, any horizontal divergence within this volume must be balanced by vertical flow through the surface A. Thus,

$$\Delta\mathrm{AMOC}_z = -\iint_A w\, dA, \tag{1}$$

where $\Delta\mathrm{AMOC}_z$ is the strength of the depth-space AMOC at RAPID minus the strength of the depth-space AMOC at OSNAP, and w is the upward velocity. Note that throughout the following sections we use the term AMOC, in the conventional way, to indicate the maximum value of the overturning streamfunction Ψ.

We can write w in Equation 1 as $w = w_e + w_r$, the sum of the Ekman pumping velocity w_e and a residual velocity w_r. The vertical Ekman pumping velocity is given by the expression

$$w_e = \nabla \times \left(\frac{\boldsymbol{\tau}_s}{\rho_0 f}\right), \tag{2}$$

where $\nabla = \left(\frac{\partial}{\partial x}, \frac{\partial}{\partial y}\right)$, $\boldsymbol{\tau}_s$ is the surface wind stress, $\rho_0 = 1027$ kg m^{-3} is a reference density, and f is the Coriolis frequency. Substituting into Equation 1 we have:

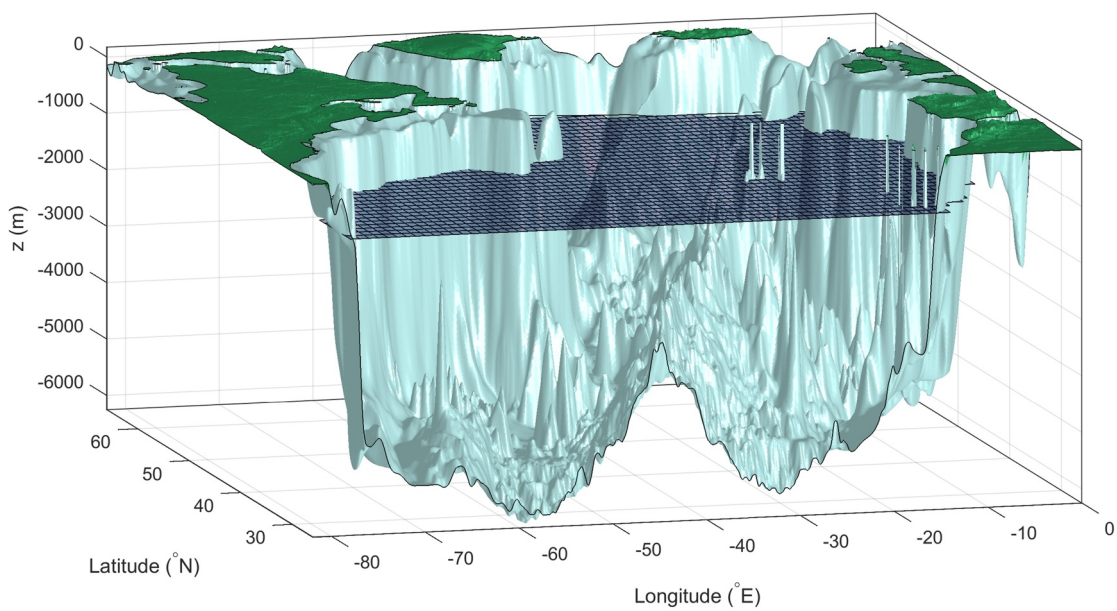

Figure 4. Schematic showing the $z = -1000$ m surface bounded by the RAPID and OSNAP sections, referred to in the text as surface A.

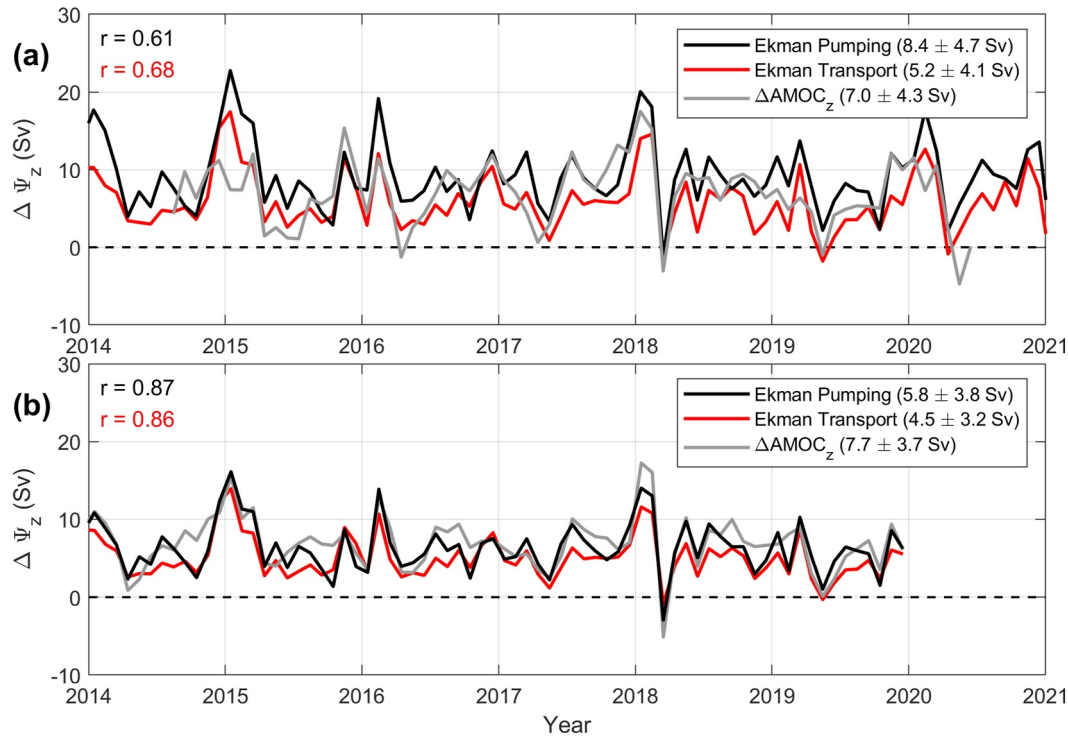

Figure 5. Time series for vertical transport from Ekman pumping integrated over the $z = -1000$ m surface bounded by the RAPID and OSNAP sections, the difference in the Ekman transport across the two sections, and the difference in the strength of the depth-space AMOC on each section. The mean ± 1 standard deviation for each time series is given in the figure legend, while the black (red) texts gives the correlation between the black (red) line and the gray line. Panel (a) shows observational results while panel (b) shows a corresponding analysis using VIKING20X model output.

$$\Delta\mathrm{AMOC}_z = -\iint_A w_e \, dA - \iint_A w_r \, dA, \tag{3}$$

In Equation 3, we compute $\Delta\mathrm{AMOC}_z$ directly from the RAPID and OSNAP observational sections. The contribution of Ekman pumping, $-\iint_A w_e \, dA$, is calculated based on $\boldsymbol{\tau}_s$ from 1/4° ERA5 reanalysis wind stress (Hersbach et al., 2020). Figure 5a shows that the vertical transport from Ekman pumping is consistent with the $\Delta\mathrm{AMOC}_z$ observed by the RAPID and OSNAP arrays. We conduct the same analysis using output from the 1/20° VIKING20X JRA55-short model hindcast of the North Atlantic (Biastoch et al., 2021; Getzlaff & Schwarzkopf, 2024) and compare their sum to $\Delta\mathrm{AMOC}_z$ diagnosed from the model horizontal velocity field (Figure 5b). In the model, the mean vertical transport from Ekman pumping is slightly lower than the mean $\Delta\mathrm{AMOC}_z$. Figure 5b shows that while the strength and variability generally agree excellently, with a correlation of $r = 0.86$, the vertical transport is consistently lower than $\Delta\mathrm{AMOC}_z$ in the autumn.

The vertical transport from Ekman pumping is closely related to the difference in the Ekman transports across the RAPID and OSNAP lines (red line in Figure 5). Using Stokes' Theorem, we can convert our area integral into a line integral which includes most of the RAPID and OSNAP sections. The difference is that our approach of integrating wind stress curl over only the region where the surface A exists omits along-shelf Ekman transports at the RAPID and OSNAP lines and includes Ekman transports between the shelf and ocean interior. While along-shelf Ekman transport will drive volume into the upper limb, this is likely balanced by shelf processes such as bottom friction and coastal pressure gradients, meaning the Ekman compensation transport occurs within the upper 1000 m. In contrast, Ekman transport across the 1000 m isobath can contribute directly to convergence above the surface A. Although this distinction makes little difference in practice, the approach of integrating wind stress curl over only the region where the surface exists will become important when tackling the AMOC in density space.

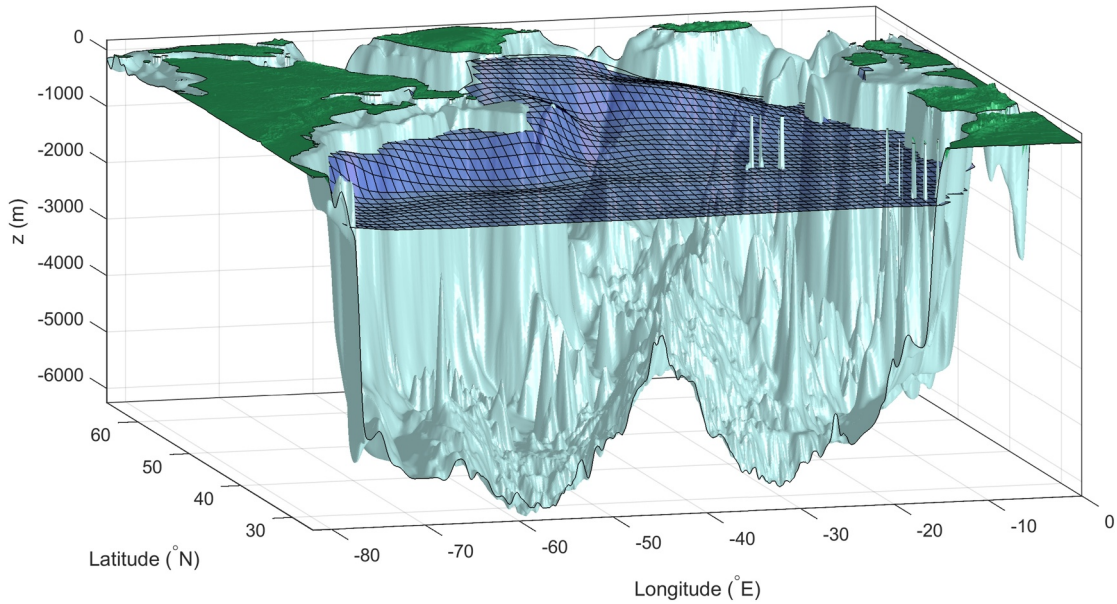

Figure 6. Schematic showing the time-mean position of the neutral surface which intersects the RAPID section at $z = -1000$ m and is bounded by the RAPID and OSNAP sections, computed from gridded EN4 hydrography. This neutral surface is referred to as surface *S*.

3. Density Space

The high level of temporal coherence between the depth- and density-space AMOC observed at OSNAP (Figure 2a), together with the near-equivalence of the depth- and density-space AMOC at RAPID (Figure 2b), suggests that the Ekman pumping mechanism upsetting meridional coherence of the AMOC in depth space also acts on the AMOC in density space. In density-space, exactly analogous to depth-space, we consider a surface *S* to be the region of the $\gamma = \gamma_0$ neutral surface bounded by the RAPID and OSNAP sections. As before, the horizontal divergence within the volume beneath the neutral surface *S* is equivalent to the meridional difference in density-space overturning stream function evaluated at $\gamma = \gamma_0$, and by volume continuity must be balanced by flow normal to that surface:

$$\Delta\Psi_{\gamma_0} = \iint_S \mathbf{u} \cdot \frac{\nabla\gamma}{|\nabla\gamma|} dS, \tag{4}$$

where $\Delta\Psi_{\gamma_0}$ is the meridional difference in density-space overturning stream function, Ψ_γ, evaluated at $\gamma = \gamma_0$. If we approximate that the density gradient, $\nabla\gamma$, is oriented vertically downward the expression becomes

$$\Delta\Psi_{\gamma_0} \approx -\iint_S w\, dS = -\iint_S w_e\, dS - \iint_S w_r\, dS, \tag{5}$$

where we have again split w into an Ekman pumping term and a residual term.

In what follows, we look to evaluate first term on the right-hand side of Equation 5 based on vertical Ekman pumping evaluated on neutral surfaces, and compare to $\Delta\Psi_{\gamma_0}$ derived from observed horizontal transports on the RAPID and OSNAP sections.

Neutral surface depths are computed using both monthly 1° gridded EN4.2.2 hydrography (Good et al., 2013) and model output based on the methods of Stanley et al. (2021). We opted to employ the orthobaric surfaces of de Szoeke et al. (2000), although our results were unchanged when using the ω-surfaces of Klocker et al. (2009). At each monthly time step, we compute the shape of the orthobaric surface γ_0 which intersects the point 26°N, 40°W, $z = -1000$ m. This location corresponds with the depth of maximum overturning in the central subtropical North Atlantic (on the RAPID line). The depth of γ_0 approximately equals -1000 m throughout the subtropics but shoals toward the western boundary and subpolar regions (Figure 6). Note that since the depth of γ_0 is zonally

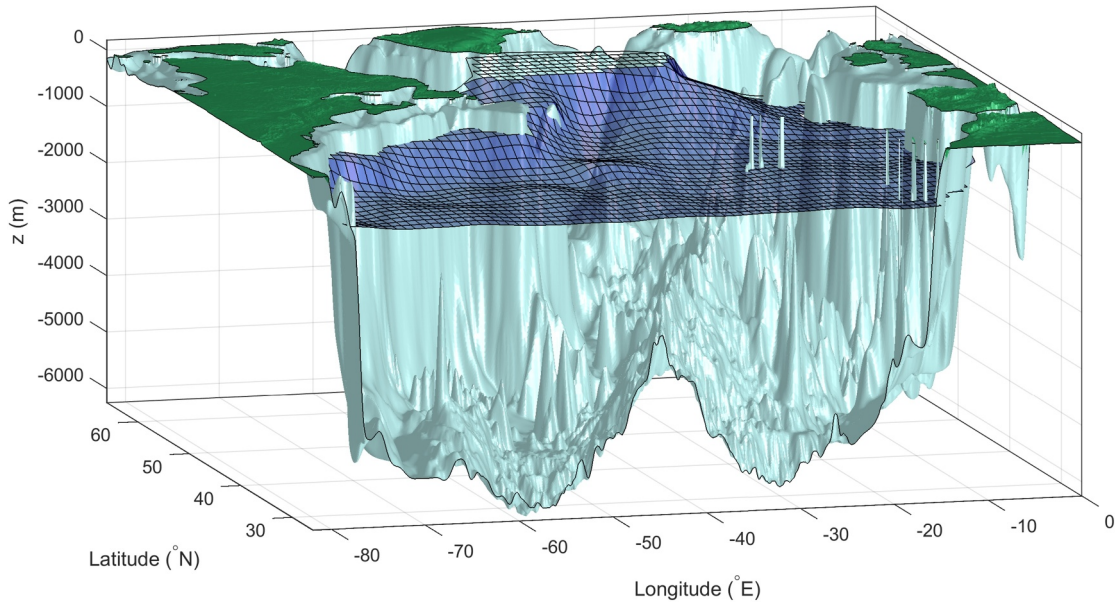

Figure 7. Schematic showing the March 2015 position of the neutral surface which intersects the RAPID section at $z = -1000$ m and is bounded by the RAPID and OSNAP arrays, computed from gridded EN4 hydrography. The open (rather than blue) hatched area shows where the surface S outcrops at the ocean surface.

uniform on the RAPID line, the choice of longitude at which we fix our surface at $z = -1000$ m is arbitrary (Figure 6). Regions where γ_0 is either grounded or outcrops at the surface, as often occurs in the winter months in the central subpolar North Atlantic (Figure 7), are omitted from our integral domain S (Equation 5). In fact, the precise depth of γ_0 is not important for our calculation; what matters is whether or not the surface exists at a given time and location.

If $\gamma = \gamma_0$ was the isopycnal of maximum overturning at two different zonal sections then $\Delta\Psi_{\gamma_0} = \Delta\text{AMOC}_\gamma$. However, as noted by Han (2023a), diapycnal fluxes in the region between RAPID and OSNAP cause the value of the isopycnal of maximum overturning to differ between the two sections. The time-mean position of $\gamma = \gamma_0$ on the OSNAP line (blue line in Figure 8a) is shallower than time-mean isopycnal of maximum overturning observed by the OSNAP array (black line in Figure 8a). To assess the effect of this meridional difference in the density of the isopycnal of maximum overturning on coherence we calculate $\Delta\Psi_{\gamma_0}$ from the RAPID and OSNAP observations using two methods. First, the density-space overturning AMOC_γ at RAPID minus that at OSNAP (i.e., ΔAMOC_γ). Second, we subtract Ψ_γ at OSNAP evaluated at the density level which corresponds best with γ_0 from AMOC_γ observed at RAPID. We refer to this difference as $\Delta\Psi_\gamma$ (dashed black line in Figure 8a). We use the observed AMOC_z as a proxy for the observed AMOC_γ at RAPID. In the corresponding model analysis, γ_0 matches the isopycnal of maximum overturning at OSNAP so closely that this distinction has no qualitative effect on the result (Figure 8b).

Figure 9a shows the time series obtained for the wind-driven component of $\Delta\Psi_{\gamma_0}$, the first term on the right hand side of Equation 5. This is compared to $\Delta\Psi_{\gamma_0}$ based on RAPID and OSNAP observations calculated using both methods described above, ΔAMOC_γ and $\Delta\Psi_\gamma$. The vertical transport from Ekman pumping is positively correlated ($r = 0.54$) with the observed meridional difference in AMOC, with the two time series each having standard deviations of 5.0 Sv. The temporal agreement is slightly better when considering $\Delta\Psi_\gamma$ (dashed line in Figure 9a), which gives a correlation of $r = 0.62$ with the Ekman pumping time series. The mean vertical transport from Ekman pumping is 8.6 Sv, whereas the mean $\Delta\Psi_\gamma$ is just 3.1 Sv, indicating that other vertical transport processes counteract Ekman pumping on longer time scales (w_r term in Equation 5). Conducting the same analysis using VIKING20X model output (Figure 9b) gives a similar agreement ($r = 0.68$) between wind-driven vertical transport and ΔAMOC_γ, which is equivalent to $\Delta\Psi_\gamma$ in the model case (Figure 8). Again, Ekman pumping drives a substantial mean downward transport which is not reflected by the mean ΔAMOC_γ. Variability in the model signal is notably suppressed compared to observations. However, given that the model is self-

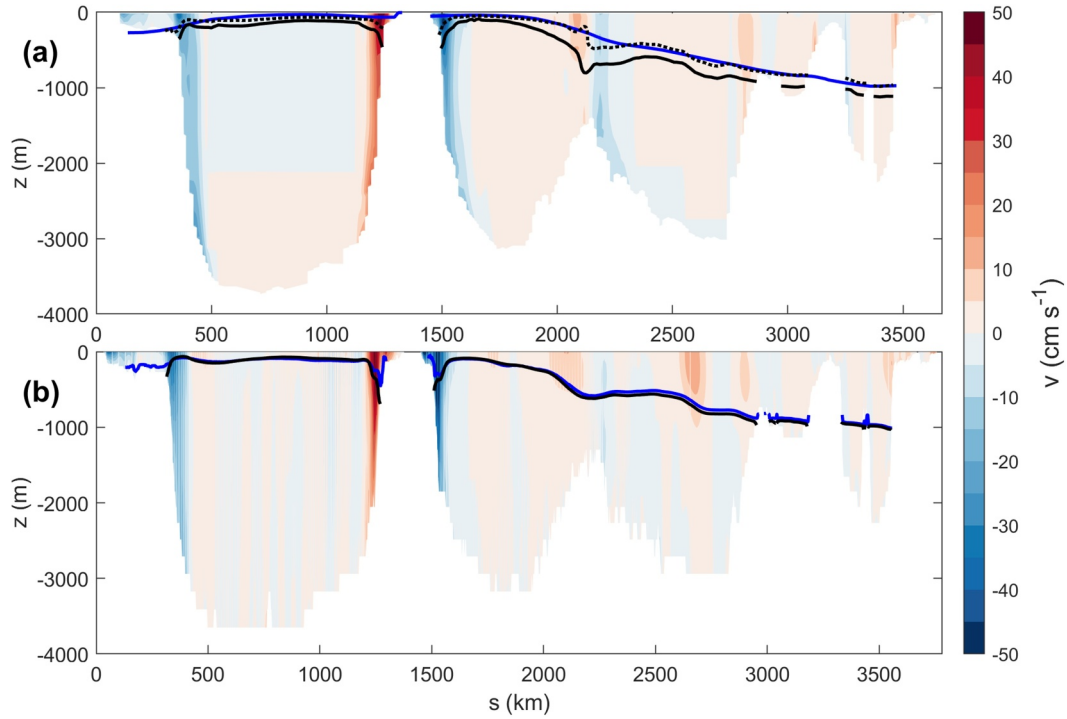

Figure 8. OSNAP cross section showing the mean depth of the neutral surface corresponding to the isopycnal of maximum overturning at RAPID (blue), the mean depth of the isopycnal of maximum overturning at OSNAP (solid black), and the isopycnal on the OSNAP line which best matches the neutral surface position (dashed black). Color scale shows mean section-normal velocity with positive flow into the page. Panel (a) shows observational results while panel (b) shows a corresponding analysis using VIKING20X model output.

consistent, these results together suggest that Ekman pumping is a critical factor in upsetting the meridional coherence of the AMOC in density space.

Other processes besides Ekman pumping can influence adiabatic isopycnal heave, such as internal Rossby waves, coastal-trapped waves, equatorial waves, and eddies (Han, 2023b). Additionally, the horizontal component of diapycnal velocity, omitted in Equation 5, might play a significant role where we have deep mixed layers. Assessing the relative importance of each of these processes is beyond the scope of this study.

4. Discussion

We have encountered compelling evidence that Ekman pumping is the dominant factor in disrupting meridional coherence of the AMOC in depth and density space. In each case, time-varying horizontal divergence is induced by fluctuations in vertical transport. The key difference is the physical interpretation of this mechanism: in depth space we have vertical transport between the upper and lower AMOC limbs, while in density space we have vertical transport changing the relative volumes of the upper and lower limbs.

Our approach does not require direct computation of isopycnal motion, as in Han (2023a). Rather, the instantaneous vertical velocity on isopycnals is inferred from the surface wind stress, while the changes in the integral domain are determined independently from gridded hydrography. This methodology is less sensitive to uncertainties in the density field within the volume bounded by the RAPID and OSNAP sections.

We have assumed that surface Ekman pumping/suction over the open ocean is balanced by horizontal divergence/convergence entirely within the AMOC lower limb. This is in contrast to the common approach of assuming Ekman compensation transport is uniformly distributed (e.g., Lee and Marotzke (1998); Hirschi and Marotzke (2007); Moat et al. (2020); Fu et al. (2023)). However, the exact location, depth and timing of surface Ekman compensation is an open question (Killworth, 2008), and depends on both seabed interaction and the

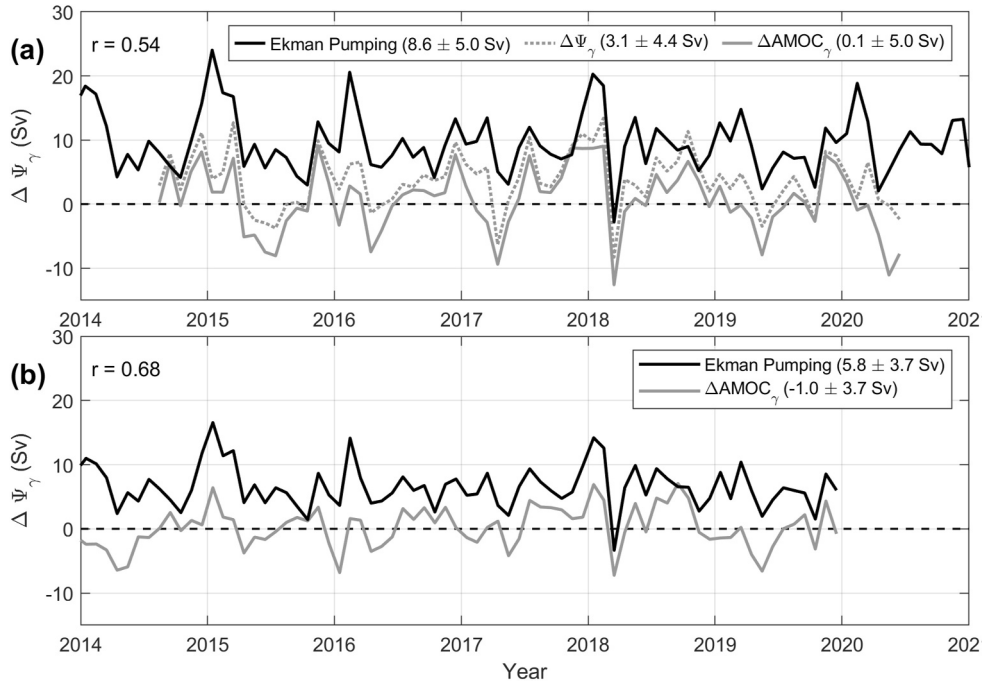

Figure 9. Time series for vertical transport from Ekman pumping integrated over the γ_0 neutral surface bounded by the RAPID and OSNAP sections, alongside the strength of the density-space AMOC at RAPID minus the strength of the density-space AMOC at OSNAP. The mean ± 1 standard deviation for each time series is given in the figure legend. Panel (a) shows observational results while panel (b) shows a corresponding analysis using VIKING20X model output. Panel (a) additionally includes the density-space AMOC at RAPID minus the overturning strength at OSNAP evaluated at the equivalent isopycnal.

conversion of vertical to geostrophic motion via the planetary β effect (Fraser et al., 2024). How this projects onto the AMOC likely depends on the thermocline depth relative to the depth/density of maximum overturning.

The temporal agreement between vertical transport from Ekman pumping and the meridional difference in AMOC does not imply that Ekman transport and AMOC are in concert on each section independently, since the Ekman transport on a given section does not necessarily produce an anomalous overturning cell. Ekman pumping anomalies will have a corresponding change in Ekman transport somewhere on the domain boundary, but the associated changes in AMOC at RAPID, for example, could in theory be caused by anomalous Ekman transport across the OSNAP line or the lateral boundaries of the domain.

While our results indicate that density-space AMOC continuity has been dominated by Ekman pumping over the last decade, changing diapycnal transports in the region between RAPID and OSNAP will likely play a substantial role on longer time scales. Previous studies (Evans et al., 2023; Petit et al., 2021) have related the mean AMOC strength in density space to diapycnal transports induced by surface buoyancy fluxes and mixing, but the effect of these diapycnal processes on AMOC variability has been obscured by the time-varying volume stored in the upper and lower AMOC limbs. Our work provides a means of accounting for this effect to gain a truer picture of how diapycnal processes characterize the density-space AMOC across different latitudes.

Data Availability Statement

This study has been conducted using E.U. Copernicus Marine Service Information (CMEMS, https://doi.org/10.48670/moi-00148). Copernicus Climate Change Service (C3S) Climate Data Store (CDS): ERA5 monthly averaged data on single levels from 1940 to present were obtained from https://doi.org/10.24381/cds.f17050d7 (Hersbach et al., 2020). Neither the European Commission nor ECMWF is responsible for any use that may be made of the Copernicus information or data it contains. EN4.2.2 data were obtained from url https://www.metoffice.gov.uk/hadobs/en4/ and are © Crown Copyright, Met Office, 2023, provided under a Non-Commercial Government License http://www.nationalarchives.gov.uk/doc/non-commercial-government-licence/version/2/

(Good et al., 2013). Data from the RAPID AMOC monitoring project is funded by the Natural Environment Research Council and are freely available from www.rapid.ac.uk/rapidmoc (Moat et al., 2020). OSNAP data were collected and made freely available by the OSNAP (Overturning in the Subpolar North Atlantic Program) project and all the national programs that contribute to it (www.o-snap.org) (Fu et al., 2023). 5-minute Gridded Global Relief Data (ETOPO5) was obtained from the National Geophysical Data Center, NOAA at http://dx.doi.org/10.7289/V5D798BF (ETOPO5, 1993). The output for the simulation VIKING20X-JRA-short is available at https://doi.org/10.26050/WDCC/VIKING20XJRAshort (Getzlaff & Schwarzkopf, 2024). Code for computing neutral surfaces is available from https://github.com/geoffstanley/neutral-surfaces (Matlab) and https://github.com/geoffstanley/neutralocean (Python) (Stanley et al., 2021).

Acknowledgments

This project was supported by the UK Natural Environment Research Council (NERC) National Capability programme CLASS NE/R015953/1, NERC grants UK-OSNAP (NE/K010875/2), UK-OSNAP-Decade (NE/T00858X/1), and SNAP-DRAGON (NE/T013494/1). This project has received funding from the European Union's Horizon 2020 research and innovation programme under grant agreement No 818123 (iAtlantic). This output reflects only the authors' view and the European Union cannot be held responsible for any use that may be made of the information contained therein. The ocean model simulation VIKING20X-JRA-short was performed at the North German Supercomputing Alliance (HLRN). The authors thank Geoff Stanley for his advice on implementing his neutral surface code. The authors also thank Lei Han and an anonymous reviewer for their thorough and insightful reviews which greatly improved the quality of this paper.

References

Biastoch, A., Schwarzkopf, F. U., Getzlaff, K., Rühs, S., Martin, T., Scheinert, M., et al. (2021). Regional imprints of changes in the Atlantic meridional overturning circulation in the eddy-rich ocean model viking20x. *Ocean Science*, *17*(5), 1177–1211. https://doi.org/10.5194/os-17-1177-2021

de Szoeke, R. A., Springer, S. R., & Oxilia, D. M. (2000). Orthoboric density: A thermodynamic variable for ocean circulation studies. *Journal of Physical Oceanography*, *30*(11), 2830–2852. https://doi.org/10.1175/1520-0485(2001)031<2830:>2.0.co;2

ETOPO5. (1993). 5-minute gridded global relief data (etopo5) [Dataset]. National Geophysical Data Center, NOAA. https://doi.org/10.7289/V5D798BF

Evans, D. G., Holliday, N. P., Bacon, S., & Le Bras, I. (2023). Mixing and air–sea buoyancy fluxes set the time-mean overturning circulation in the subpolar north Atlantic and Nordic seas. *Ocean Science*, *19*(3), 745–768. https://doi.org/10.5194/os-19-745-2023

Fraser, N. J., Fox, A. D., Cunningham, S. A., Rath, W., Schwarzkopf, F. U., & Biastoch, A. (2024). Vertical velocity dynamics in the north Atlantic and implications for amoc. *Journal of Physical Oceanography*, *54*(9), 2011–2024. https://doi.org/10.1175/JPO-D-23-0229.1

Fu, Y., Lozier, M. S., Biló, T. C., Bower, A. S., Cunningham, S. A., Cyr, F., et al. (2023). Seasonality of the meridional overturning circulation in the subpolar north Atlantic. *Communications Earth & Environment*, *4*(181), 181. https://doi.org/10.1038/s43247-023-00848-9

Getzlaff, K., & Schwarzkopf, F. U. (2024). viking20x-jra-short: Daily to multi-decadal ocean dynamics under jra55-do atmospheric forcing [Dataset]. *World Data Center for Climate (WDCC) at DKRZ*. https://doi.org/10.26050/WDCC/VIKING20XJRAshort

Good, S. A., Martin, M. J., & Rayner, N. A. (2013). en4: Quality controlled ocean temperature and salinity profiles and monthly objective analyses with uncertainty estimates [Dataset]. *Journal of Geophysical Research: Oceans*, *118*(12), 6704–6716. https://doi.org/10.1002/2013JC009067

Han, L. (2023a). Exploring the amoc connectivity between the rapid and osnap lines with a model-based data set. *Geophysical Research Letters*, *50*(19), e2023GL105225. https://doi.org/10.1029/2023gl105225

Han, L. (2023b). Mechanism on the short-term variability of the Atlantic meridional overturning circulation in the subtropical and tropical regions. *Journal of Physical Oceanography*, *53*(9), 2231–2244. https://doi.org/10.1175/JPO-D-23-0027.1

Hersbach, H., Bell, B., Berrisford, P., Hirahara, S., Horányi, A., Muñoz-Sabater, J., et al. (2020). The era5 global reanalysis [Dataset]. *Quarterly Journal of the Royal Meteorological Society*, *146*(730), 1999–2049. https://doi.org/10.1002/qj.3803

Hirschi, J., & Marotzke, J. (2007). Reconstructing the meridional overturning circulation from boundary densities and the zonal wind stress. *Journal of Physical Oceanography*, *37*(3), 743–763. https://doi.org/10.1175/JPO3019.1

Killworth, P. D. (2008). A simple linear model of the depth dependence of the wind-driven variability of the meridional overturning circulation. *Journal of Physical Oceanography*, *38*(2), 492–502. https://doi.org/10.1175/2007JPO3811.1

Klocker, A., McDougall, T. J., & Jackett, D. R. (2009). A new method for forming approximately neutral surfaces. *Ocean Science*, *5*(2), 155–172. https://doi.org/10.5194/os-5-155-2009

Lee, T., & Marotzke, J. (1998). Seasonal cycles of meridional overturning and heat transport of the Indian ocean. *Journal of Physical Oceanography*, *28*(5), 923–943. https://doi.org/10.1175/1520-0485(1998)028¡0923:SCOMOA¿2.0.CO;2

Moat, B. I., Smeed, D. A., Frajka-Williams, E., Desbruyères, D. G., Beaulieu, C., Johns, W. E., et al. (2020). Pending recovery in the strength of the meridional overturning circulation at 26° n. *Ocean Science*, *16*(4), 863–874. https://doi.org/10.5194/os-16-863-2020

Petit, T., Lozier, M. S., Josey, S. A., & Cunningham, S. A. (2021). Role of air-sea fluxes and ocean surface density in the production of deep waters in the eastern subpolar gyre of the north Atlantic. *Ocean Science*, *17*(5), 1353–1365. https://doi.org/10.5194/os-17-1353-2021

Stanley, G. J., McDougall, T. J., & Barker, P. M. (2021). Algorithmic improvements to finding approximately neutral surfaces. *Journal of Advances in Modeling Earth Systems*, *13*(5), e2020MS002436. https://doi.org/10.1029/2020MS002436